Elevated temperature creep properties of NiAl cryomilled with and without Y_2O_3

J. Daniel Whittenberger[a)]
NASA Lewis Research Center, Cleveland, Ohio 44135

Michael J. Luton
Exxon Research and Engineering, Annadale, New Jersey 08801

(Received 27 June 1994; accepted 30 January 1995)

The creep properties of lots of NiAl cryomilled with and without Y_2O_3 have been determined in compression and tension. Although identical cryomilling procedures were used, differences in composition were found between the lot ground with 0.5 vol% yttria and the lot ground without Y_2O_3. Compression testing between 1000 and 1300 K yielded similar creep strengths for both materials, while tensile creep rupture testing indicated that the yttria-containing alloy was slightly stronger than the Y_2O_3-free version. Both compression and tensile testing showed two deformation regimes; whereas the stress state did not affect the high stress exponent ($n \approx 10$) mechanism, the low stress exponent regime n was ~6 in tension and ~2 in compression. The strengths in tension were somewhat less than those measured in compression, but the estimated activation energies (Q) of ~600 kJ/mol for tensile testing were closer to the previously measured values (~700 kJ/mol) for NiAl–AlN and very different from the Q's of 400 and 200 kJ/mol for compression tests in the high and low stress exponent regimes, respectively. A Larson–Miller comparison indicated that cyromilling can produce an alloy with long-term, high-temperature strength at least equal to conventional superalloys.

I. INTRODUCTION

High energy milling of the B2 crystal structure intermetallic NiAl in liquid N has been identified as an effective technique to impart high temperature strength in this aluminide.[1–10] Such processing, generically termed cryomilling,[11,12] leads to the formation of a thin mantle containing extremely fine AlN precipitates around each NiAl powder particle.[13] During subsequent elevated temperature densification procedures (for example, hot isostatic pressing or extrusion), powder particles are welded together to yield a cellularlike microstructure, where AlN-enriched cell walls encircle nitride deficient cell interiors. Typically the AlN-reinforced aluminide exhibits a factor of 6 increase in creep strength over that demonstrated by polycrystalline NiAl.[10]

While the reproducibility of the cryomilling process in terms of mechanical strength has been verified by milling different heats of prealloyed NiAl powder[5] and multiple trials on the same heat of powder,[9] the oxidation resistance of various batches of NiAl–AlN has been problematic. For instance, the first lot of AlN-reinforced material, which was milled with a 0.5 wt.% Y_2O_3 addition, was shown to have excellent oxidation properties[14]; indeed, the behavior of this alloy nearly equaled the best third element doped NiAl. However, subsequent cryomilling,[5] which was accomplished without yttria, yielded materials with decidedly poorer oxidation resistance than the initial lot of NiAl–AlN.[15] As the most likely explanation for this discrepancy lies in the presence/absence of yttria, an experiment to test this hypothesis was undertaken. Specifically, two lots of NiAl powder were cryomilled under identical conditions with the exception that one lot was milled with Y_2O_3 and the other was not. Subsequent oxidation testing of these materials[10] conclusively demonstrated that yttria does improve the oxidation resistance.

Concurrent with the oxidation study, the elevated temperature compressive and tensile creep strengths of yttria-free and yttria-containing AlN particulate strengthened NiAl's were also determined. This paper describes the results of mechanical property testing between 1000 and 1300 K on materials that have been densified by hot extrusion.

II. EXPERIMENTAL PROCEDURES

Cryomilling of NiAl powder was undertaken at Exxon Research and Engineering (Annadale, NJ). The starting prealloyed NiAl powder was the same heat (P541, Homogeneous Metals, Inc., Table I) as utilized in the initial work.[1–4] A modified Model 1–S Szegvari

[a)]Currently at Max-Planck-Institut für Metallforschung, Institut für Werkstoffwissenschaft, Stuttgart, Germany.

TABLE I. Chemical analysis (wt. %) of NiAl cryomilled with and without Y_2O_3.

ID	Extrusion conditions		Elements						
	Tooling (billet) diameter	Reduction in area	Al	C	Ni	N	O	Y	Major impurities
As gas atomized powder	...	...	31.88	0.002	68.39	<10 wppm	0.009	...	0.1 Fe[a]
Without Y_2O_3									
As cryomilled powder	...	...	30.53	0.014	65.38	1.95	0.51	...	0.1 Fe[a]
Ohne	51 mm	8 : 1	30.70	0.005	66.08	1.96	0.47	...	0.1 Fe[a]
Ohne-I	76 mm	8 : 1	31.01	0.011	66.22	2.00	0.53	...	0.1 Fe[a]
Ohne-II	76 mm	12 : 1	30.62	0.010	65.28	2.10	0.48	...	0.1 Fe[a]
With Y_2O_3									
As cryomilled powder	...	...	31.12	0.015	66.17	1.48	0.50	0.35	0.1 Fe[a]
Mit	51 mm	8 : 1	30.97	0.005	66.18	1.56	0.46	0.35	<0.1 Fe[a]
Mit-I	76 mm	8 : 1	31.10	0.022	66.36	1.56	0.48	0.36	0.1 Fe[a]
Mit-II	76 mm	12 : 1	30.76	0.021	65.34	1.60	0.49	0.35	<0.15 Fe[a]

[a]B, Ba, Ca, Co, Cr, Cu, Mg, Mn, Mo, Na, Nb, Si, Ti, V, Zn, and Zr less than 0.5 wppm.

10 l attritor was used for cryomilling, where the attritor main shaft rotated at 180 rpm, while liquid nitrogen was continuously introduced into the milling chamber to maintain the level of the grinding ball/powder/liquid nitrogen slurry above the upper attritor arm. Two lots of NiAl were milled under identical conditions with the exception that one lot was doped with a 0.5 wt. % Y_2O_3 addition (<10 μm diameter particles from Research Chemicals) while the other lot was ground without yttria. At the completion of the 16 h runs, the mill was allowed to warm to room temperature under dry Ar, and the cryomilled powder was subsequently handled in air.

Both lots of powder were densified under several different extrusion conditions at 1505 K. For the initial attempt approximately 220 g of powder were vacuum sealed in 51 mm diameter, 6.3 mm thick wall mild steel cans and hot extruded at an 8 : 1 reduction ratio. After the successful densification of both lots by this procedure, larger steel cans (76 mm diameter, 6.3 mm wall) were filled with ~600 g of cryomilled powder, evacuated, and sealed. Since the 1505 K 8 : 1 extrusion of each composition was then accomplished with plenty of remaining press capacity, the reduction ratio was increased to 12 : 1 and the last two 76 mm cans were extruded at this higher reduction ratio. While hot extrusion was successful in densifying the cryomilled NiAl, it should be noted that the yield was not 100%. Because of the extreme difference in strength between the aluminide and mild steel at 1505 K, in some instances the can wall thinned to the point where NiAl was directly exposed to air upon passing through the minimum die diameter. This caused cracks in the aluminide and the loss of some material.

Because the primary reason for the original work was to establish the role of yttria on oxidation resistance, the majority of the usable material from the 8 : 1 extruded bars was used for the oxidation experiments.[10,15] The remaining 8 : 1 and all the 12 : 1 extruded stock was then cut into mechanical properties samples. Cylindrical compression specimens were wire electrodischarge machined (EDM) to final size, ~5 mm in diameter by about 10 mm in length, from the as-extruded bar with the length of the samples parallel to the extrusion axis. Tensile specimen blanks, ~7 mm in diameter by ~50 mm long, were also EDM from the extruded bars. The blanks were then centerless ground into cylindrical buttonhead tensile type samples with a 3.2 mm diameter by 30 mm gage section.

Compressive properties were measured in air between 1000 and 1300 K, utilizing two different procedures. Stress-strain behavior at strain rates ranging from about 2×10^{-4} to 2×10^{-7} s^{-1} was determined in a universal test machine running under constant crosshead velocity conditions, where the autographically recorded load-time charts were converted to true compressive stresses, strains, and strain rates via the offset method and the assumption of conservation of volume. Constant load compressive creep testing was undertaken in lever arm test machines, where deformation was determined as a function of time via a linear variable differential transducer (LVDT) connected to a data acquisition system that measured the relative positions of ceramic

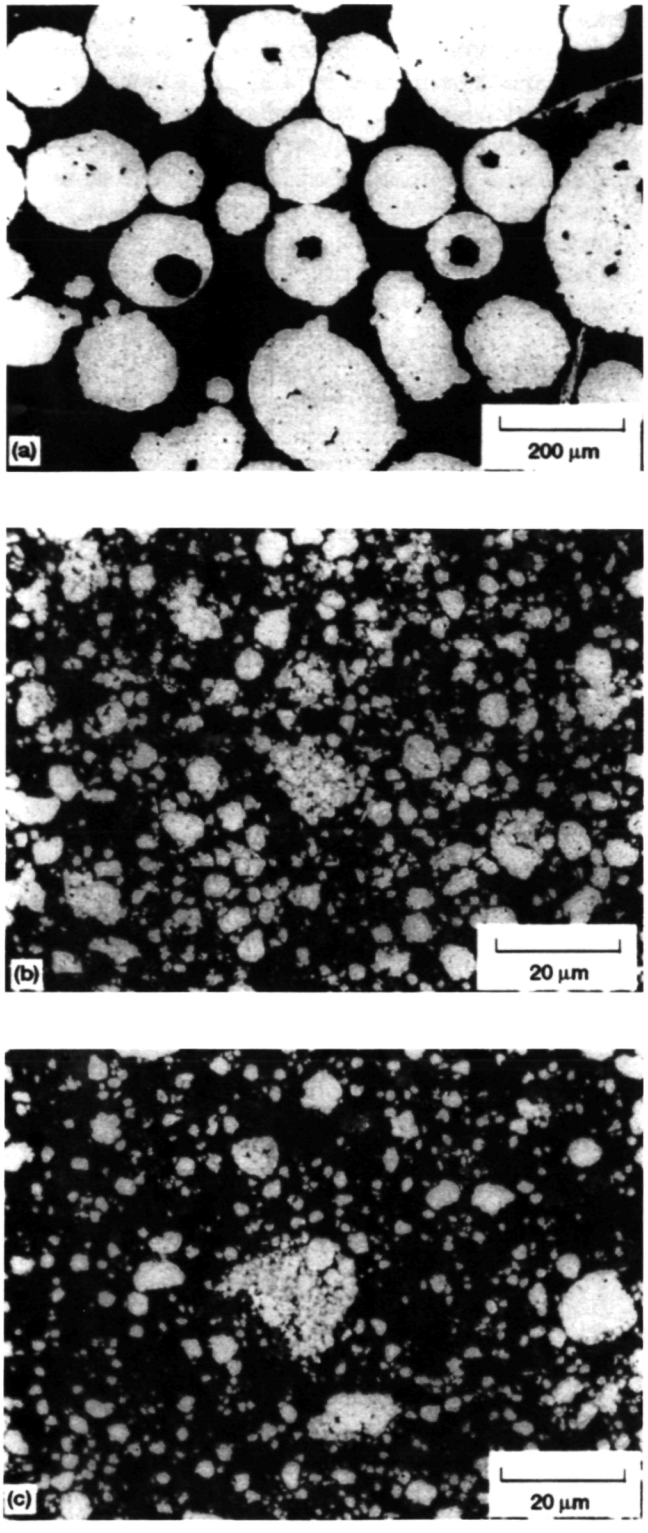

FIG. 1. Light optical photomicrographs of the NiAl powders: as received (a) and after cryomilled with yttria (b) and without yttria (c).

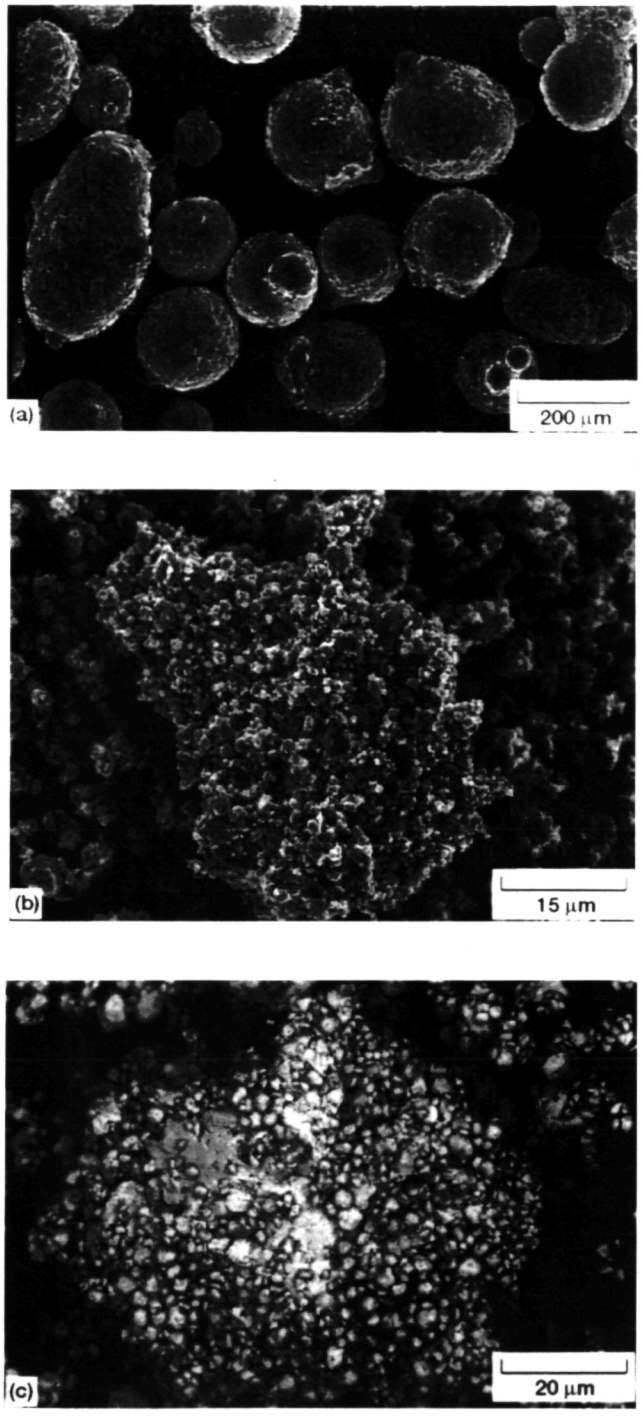

FIG. 2. SEM photomicrographs of the NiAl powders: as received (a) and after cryomilled with yttria (b) and without yttria (c).

push bars applying the load to the specimen. Such information was normalized with respect to the final specimen length and converted into true stress and strains by assuming volume conservation. In order to maximize the compressive creep data, many of the specimens were subjected to multiple stress testing where the applied load was always increased during the experiment.

Tensile creep behavior was measured in air between 1100 and 1300 K utilizing constant load lever arm test frames and superalloy load trains equipped with split collar grips. Sample elongation was measured through

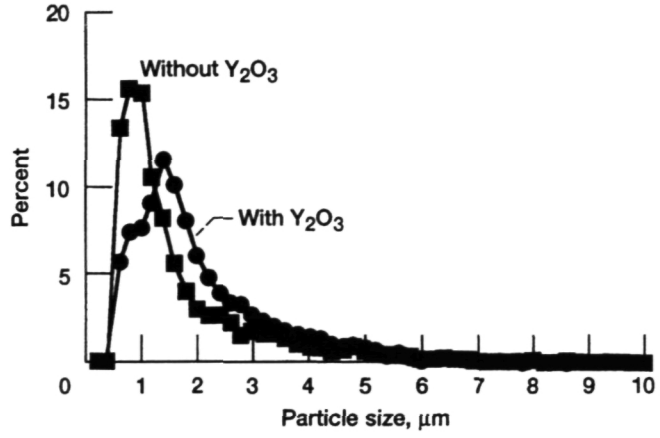

FIG. 3. Particle size distributions for NiAl cryomilled with and without Y_2O_3.

an extensometer that was attached to each specimen grip by three cone-pointed set screws. Separation of the grips was then tracked by a LVDT connected to a data acquisition system. The resultant voltage-time data were transformed to creep curves, assuming that all the relative motion of the extensometer was due to strain in the specimen gage. All uniaxial tensile creep tests were conducted to failure under a constant engineering stress.

The as-received prealloyed powder, the cryomilled powders, and hot extruded bar stock were characterized by standard chemical analysis, x-ray diffraction, scanning electron microscopy (SEM), and metallographic techniques. Results from these efforts are reported in this paper. Post-test microstructural studies, including transmission electron microscopy, of the compression

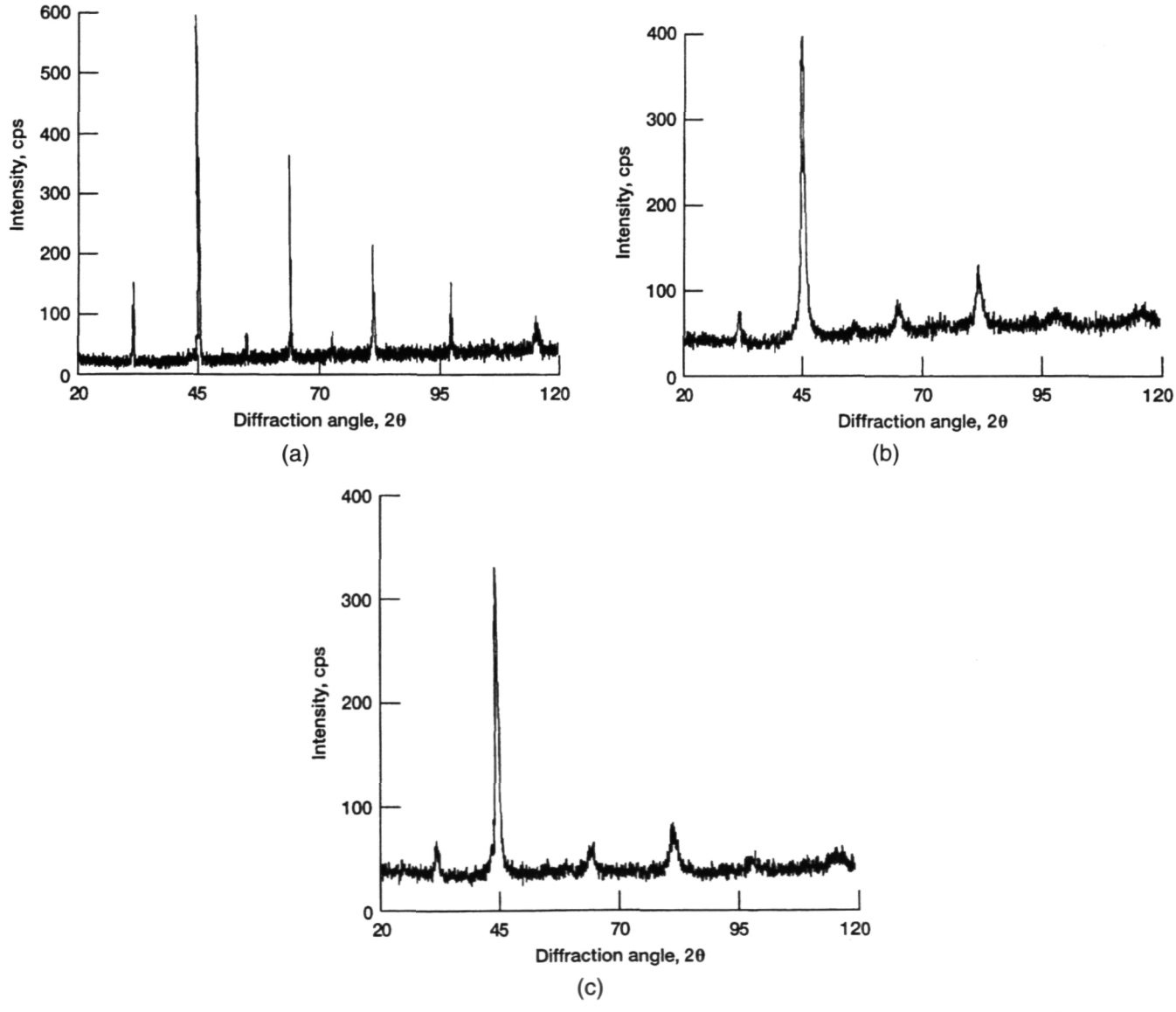

FIG. 4. X-ray diffraction patterns for various NiAl powders irradiated with Cu K_α: (a) as received, (b) cryomilled with Y_2O_3, and (c) cryomilled without Y_2O_3.

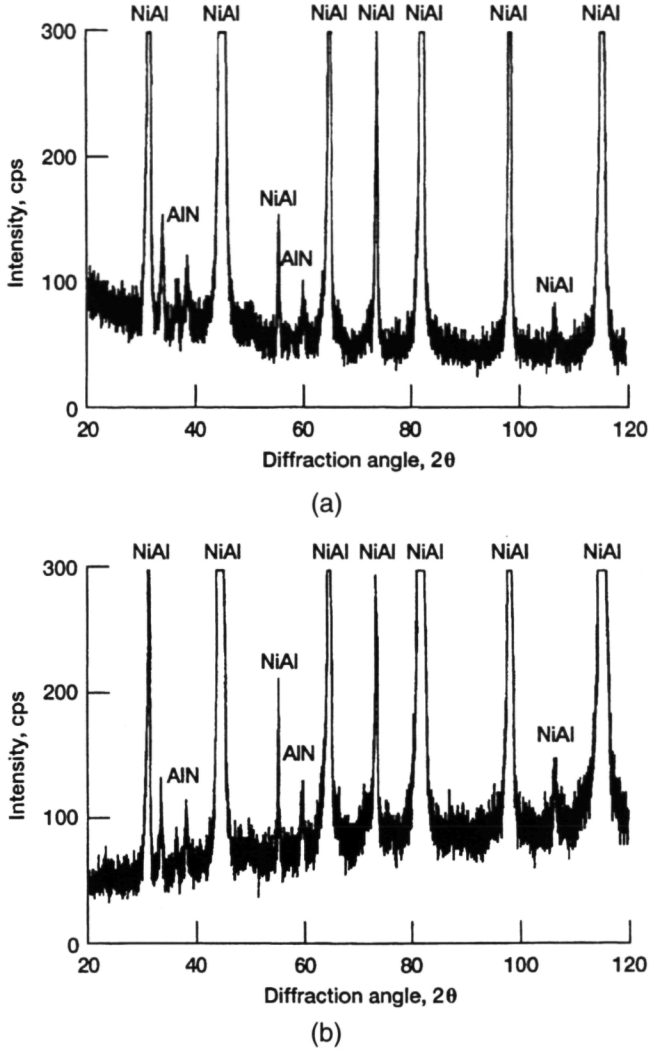

FIG. 5. X-ray diffraction patterns for cryomilled NiAl after being hot extruded from 76 mm tooling at 1505 and a 8 : 1 reduction ratio; samples irradiated with Cu K_α: (a) cryomilled with Y_2O_3 and (b) cryomilled without Y_2O_3.

and tension samples are currently underway and will be reported elsewhere.

III. RESULTS

A. Materials

Although the prealloyed NiAl powder utilized in this study and the original cryomilling experiment[1] were from the same heat, the powder utilized in Ref. 1 had a uniform, ~60 μm diameter spherical shape,[3] while, as can be visualized in the light optical cross sections {Fig. 1(a) and the SEM photomicrograph of the surfaces [Fig. 2(a)]}, the current starting powder was much larger (~150 to 200 μm) and somewhat irregular in shape. After cryomilling, the dimensions of the product [Figs. 1(b) and 1(c)] were much smaller than the as-received NiAl powder. Particle size/distributions measured by laser light techniques (Fig. 3) indicated that the log-normal mode of NiAl cryomilled with yttria (1.57 μm) was greater than that (1.10 μm) for the lot milled without Y_2O_3; however, these values were not statistically different. The cross sections [Figs. 1(b) and 1(c)] and exterior surfaces of both lots of cryomilled particles were similar in shape, ranging from irregular oblongs to near spheres and sizes ranging from ~0.5 to ~10 μm in diameter. For the most part, the larger particles appeared to be aggregates of smaller particles [Figs. 2(b) and 2(c)].

Results of x-ray diffraction analyses of the powders before and after cyromilling are presented in Fig. 4. The as-received material [Fig. 4(a)] exhibited a low background level and sharp peaks corresponding to a lattice parameter (a_0) for NiAl of 0.2884 ± 0.0002 nm. After cryomilling, the background level had risen [Figs. 4(b) and 4(c)], and only diffraction peaks ascribable to NiAl were visible. These became somewhat broader and less intense in comparison to the as-received powder [Fig. 4(a)]; hence, the NiAl lattice parameter estimates were less accurate {0.289 nm for the lot containing Y_2O_3 [Fig. 4(b)] and 0.287 nm for the yttria-free lot [Fig. 4(c)]}, and the uncertainty has increased an order of magnitude to ~0.002 nm. After hot extrusion of the cryomilled powders, the x-ray patterns (Fig. 5) indicated the presence of AlN in the NiAl matrix. Additionally, the thermomechanical processing had sharpened the aluminide peaks which permits a more refined estimate of the lattice parameters which are about 0.2885 ± 0.0002 nm for both lots.

Concurrent with the appearance of AlN in the x-ray diffraction patterns, the distinctive cellular microstructure was developed in the hot extruded materials (Fig. 6). The most prominent features at the low magnifications [Figs. 6(a) and 6(b)] were the irregular cross-section cigar-shaped "grains", elongated in the extrusion direction, which are surrounded by AlN particles. At higher magnifications [Figs. 6(c) and 6(d)] it can be seen that in some regions the nitrides outline areas devoid of second phases, while in other regions the AlN particles are more or less uniformly dispersed. For purposes of characterization, the AlN-free areas form the "cell interiors" or "cores" of the microstructure, while the AlN-rich regions form the "cell walls" or "mantle" portion of the structure. As is illustrated in Figs. 6(c) and 6(d), a large distribution in AlN particle diameters exists within the mantle with sizes ranging from a few microns downward.

Chemical compositions of all the materials in various stages of processing are given in Table I. In particular, the as-received, gas-atomized powder had very low interstitial contents of approximately 20 wppm C, <10 wppm N, and 90 wppm O. After cryomilling, the carbon content in both lots had increased somewhat to about 150 wppm, while the amounts of N and O had dramatically changed from wppm levels to wt. % values.

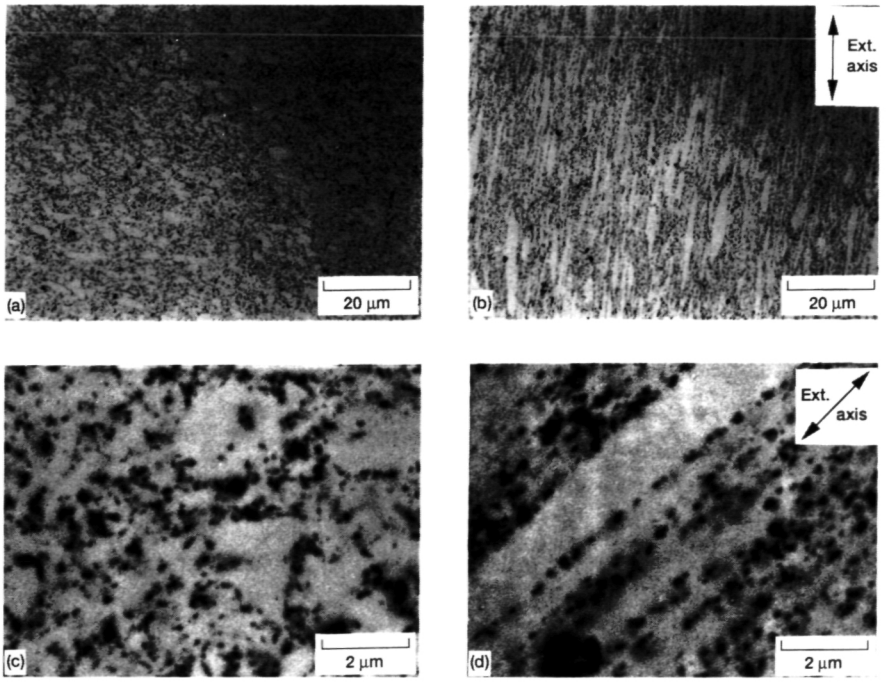

FIG. 6. Typical unetched microstructure in hot extruded cryomilled NiAl as revealed by light optical (a, b) and back scatter SEM (c, d) techniques. Material was extruded at 1505 K at 12 : 1. (a) and (c) are cross sections and (b) and (d) are longitudinal sections.

There was a clear difference in the N content in the two lots of cryomilled NiAl, where the powder milled with Y_2O_3 contains about 25% less N than the powder milled without yttria. In addition, both lots had the same O content after cryomilling, even though the lot ground with yttria started with ~0.2 wt. % O from the Y_2O_3 addition. The difference in N levels and consistency in O content between the two lots was verified through analysis of the extruded stock (Table I). Furthermore, the concentrations of Al, C, N, O, and Ni measured for the three densified bars from each lot are in good agreement with each other as well as that determined for the as-cryomilled powder.

The chemistries reported in Table I were used to estimate the Al content of the NiAl matrix and the volume fractions of second phases. This calculation was made with the following assumptions: (i) All N forms AlN with a density of 3.27 Mg/m^3; (ii) all Y remains in the form of Y_2O_3 with a density of 5.01 Mg/m^3; (iii) the O in excess to that required to produce Y_2O_3 is in the form of Al_2O_3 with a density of 3.97 Mg/m^3; (iv) low levels of iron (Table I) have essentially no effect on the density of NiAl; and (v) all C forms an interstitial solid solution in NiAl. As expected from the closeness of the overall chemistries (Table I), conformity [Table II(a)] existed in the matrix Al contents and volume fractions of nitride and oxide among the various forms for each lot of cryomilled NiAl. Hence, average compositions and standard deviations for each lot of cryomilled powder, independent of consolidation condition, are given in Table II(b). In round numbers the lot of NiAl cryomilled with yttria has a Ni–47.5Al matrix with about 8.1 vol % AlN, 1.2 vol % Al_2O_3, and 0.5 vol % Y_2O_3, while the lot milled without yttria has a slightly lower matrix Al content and higher amounts of nitride and oxide: Ni–46.5Al + 10.5 vol % AlN + 1.6 vol % Al_2O_3. Overall, chemical analysis (Tables I and II) indicated several important factors; in particular, the data show that the chemistry is uniform and reproducible and that thermomechanical processing of the cryomilled powder by hot extrusion has no effect on the composition.

The current observations for as-cryomilled powders and the resultant extruded product are similar to those drawn in Refs. 1–3, 9, 10, and 13. Specifically, cryomilling simultaneously fragments the NiAl powder, while a surface reaction leads to the formation of AlN in a thin surface layer. The nitrides in the as-cryomilled powder are not visible by x-ray techniques, but hot extrusion promotes growth of the AlN particles and results in cigar-shaped, particle-free grains outlined by small nitrides. Although the lot cryomilled with Y_2O_3 had ~25% less N than the lot milled without yttria, it is not certain that this is a real difference ascribable to the yttrium oxide. Previous examination[9] of four heats of NiAl cryomilled without Y_2O_3 under

TABLE II. Matrix composition and second phase content of NiAl cryomilled with and without Y_2O_3.

	Matrix composition, at. %				Volume fraction second phases (%)		
	Al	C	Fe	Ni	AlN	Al_2O_3	Y_2O_3
(a) Individual values							
As gas atomized powder	50.31	0.007	0.076	49.61	...	...	...
Without Y_2O_3							
As cyromilled powder	46.52	0.056	0.086	53.34	10.3	1.61	...
Ohne	46.45	0.02	0.085	53.44	10.27	1.47	...
Ohne-I	46.55	0.043	0.085	53.33	10.41	1.65	...
Ohne-II	46.4	0.04	0.086	53.47	11.05	1.51	...
With Y_2O_3							
As cryomilled powder	47.7	0.058	0.083	52.15	7.71	1.26	0.5
Mit	47.49	0.019	0.083	52.4	8.14	1.14	0.5
Mit-I	47.49	0.085	0.083	52.35	8.11	1.19	0.5
Mit-II	47.46	0.082	0.13	52.33	8.42	1.25	0.5
(b) Average values							
Without Y_2O_3							
Average	46.48	0.04	0.09	53.40	10.51	1.56	...
Standard deviation	0.06	0.01	...	0.06	0.32	0.07	...
With Y_2O_3							
Average	47.54	0.06	0.09	52.31	8.10	1.21	0.5
Standard deviation	0.10	0.03	0.02	0.09	0.25	0.05	...

identical conditions resulted in a 20% relative range in N content.

B. Mechanical properties

1. Compression testing

Sufficient material was available to obtain compression samples from the 76 mm tooling, 12 : 1-1505 K extrusion of the lot milled without yttria (identified as "Ohne-II", Table I) and both the 8 : 1 and 12 : 1, 76 mm tooling extrusions of the lot milled with Y_2O_3 (identified as "Mit-I" and "Mit-II", respectively, Table I). Examples of the true stress-strain curves obtained under constant velocity conditions are presented in Fig. 7(a) for Mit-II and Ohne-II tested at 1300 K and in Fig. 7(b) for Mit-I tested between 1000 and 1200 K. These materials exhibited similar stress-strain diagrams irrespective of the imposed strain rate or temperature, where work hardening occurs during the initial ~1.5% strain and is followed by continuous flow at a more or less constant stress. At a constant temperature, the steady-state flow stresses decreased with a decreasing strain rate [Figs. 7(a) and 7(b)], and for a constant strain rate the flow stresses decreased with increasing temperature [Fig. 7(b)].

Examples of constant load compression creep results are given in Fig. 8 as a function of engineering stress for Mit-II tested between 1000 and 1300 K. Because of the limited number of available samples, most specimens were subjected to multistress experiments. At all test temperatures, application of initial stress and/or stress jumps result in normal primary creep with a decreasing instantaneous creep rate followed by steady-state deformation. Similar behavior was observed for both Mit-I and Ohne-II.

The true compressive flow stress (σ) strain rate ($\dot{\epsilon}$) data for the various materials are summarized in Fig. 9, where stress and strain rate were evaluated at 3% strain from the constant velocity tests (for example, Fig. 7) and values from the steady state were taken from the constant load tests (for example, Fig. 8). Based on the negligible scatter in the data for the various materials and densification conditions, there appeared to be little difference in strength among Mit-I, Mit-II, and Ohne-II tested between 1000 and 1300 K. However, there seemed to be at least three separate deformation regimes, where the slope at 1300 K for strain rates

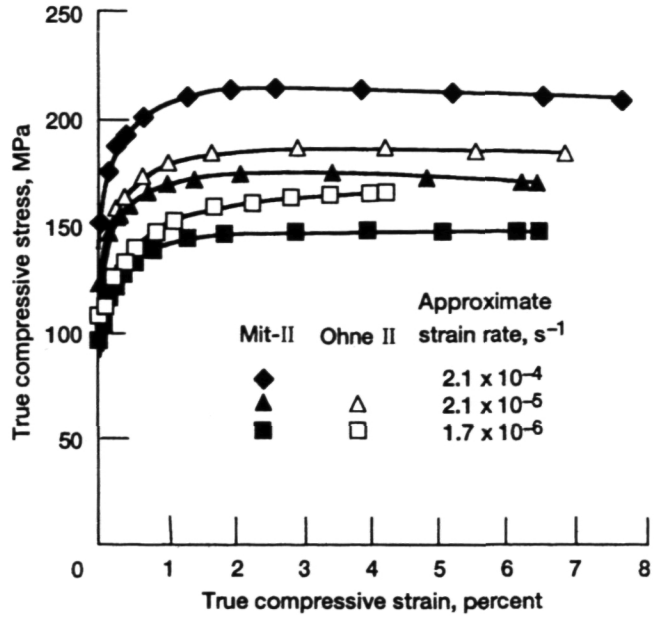

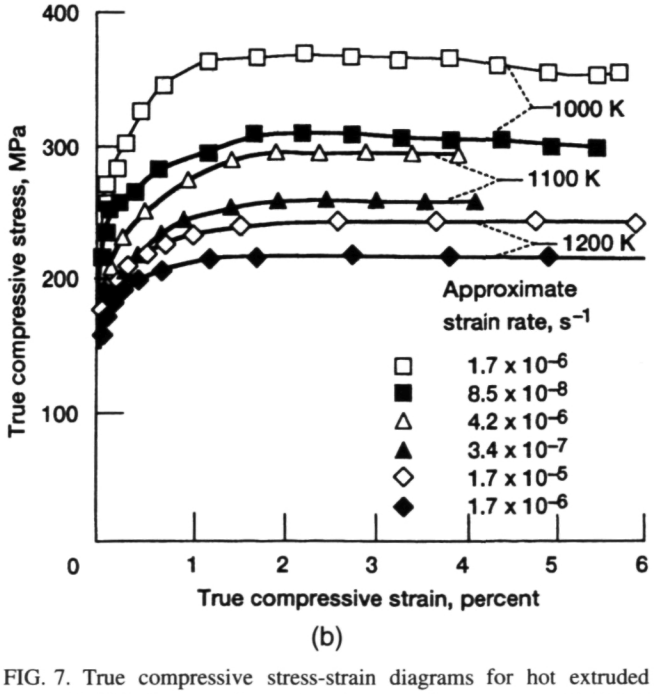

FIG. 7. True compressive stress-strain diagrams for hot extruded cryomilled NiAl as functions of strain rate and temperature. (a) Mit-II and Ohne-II tested at 1300 K. (b) Mit-I tested between 1000 and 1200 K.

$>10^{-8}$ s^{-1} is different than the slope for 1000 to 1200 K testing; likewise, the slope of the data for the lowest strain rate experiments at 1100 to 1300 K is significantly changed from that of the higher strain rate tests. These separations can be best visualized through use of the standard temperature-compensated power-law equation to define the extent of each regime. To this end, all appropriate stress-strain rate values were fitted by linear regression techniques to

$$\dot{\epsilon} = B\sigma^n \exp\left(\frac{-Q}{RT}\right), \quad (1)$$

where B is a constant in s^{-1}, n is the stress exponent, Q is the apparent activation energy, R is the universal gas constant, and T is the temperature. The stress exponents, activation energies, and appropriate statistical parameters, including the standard deviations for stress exponents $\{\delta_n\}$ and activation energy $\{\delta_Q\}$ and coefficient of determination $\{R_d^2\}$, are listed in Table III.

Initial fitting to Eq. (1) involved the use of a dummy variable to test for differences among the three materials. This procedure began with comparison of Mit-I and Mit-II data and then continued with the contrasting of pooled Mit-I + Mit-II values to those of Ohne-II. No statistically significant differences were found for either situation in any of the three regimes; hence, the data for all materials were joined and fitted to Eq. (1). The three sets of lines that describe the overall compressive behavior of Mit-I, Mit-II, and Ohne-II are shown in Fig. 9. These curves clearly define the limits of each of the three regimes, where (i) the 1000–1200 K higher stress results can be quantified by a very high stress exponent ($n = 14.4$) and ~400 kJ/mol activation energy, (ii) the 1300 K data for $\epsilon > 10^{-8}$ s^{-1} is best described by a somewhat lower n value (10.3), and (iii) the lowest stress tests at 1100–1300 K indicate a very low stress exponent ($n = 2$) and an activation energy (Q of ~200 kJ/mol) half that of the higher stress 1000–1200 K behavior.

The 1300 K behavior of the current lots of NiAl–AlN is contrasted to that of the first heat of cryomilled nickel aluminide containing 10.3 vol% AlN[1–4,10] and polycrystalline NiAl[16] in Fig. 10. Comparisons at lower temperatures were not possible, since only three flow stress-strain rate values[1] exist for the original NiAl–AlN tested below 1300 K. Clearly, cryomilling improved the elevated temperature strength of NiAl, as witnessed by the small portion of the $\sigma - \dot{\epsilon}$ curve for unreinforced NiAl shown in the upper left-hand corner of this figure. However, the behavior of Mit-I, Mit-II, and Ohne-II was different from that displayed by the original NiAl–AlN and other previously manufactured lots of cryomilled NiAl–AlN.[5,9] In particular, the first material displayed a clear transition at ~10^{-7} s^{-1} (Fig. 10) from a high stress exponent regime ($n = 13.1$) to an intermediate stress exponent mechanism ($n = 5.6$), which is similar to that of polycrystalline NiAl.[16] On the other hand, the current heats exhibited a stress exponent change from 10.3 to 2 at about 10^{-8} s^{-1} (Fig. 10).

Concurrent with the differences in stress exponents, significant disagreement in the measured activation energies was found. For example, the original heat of

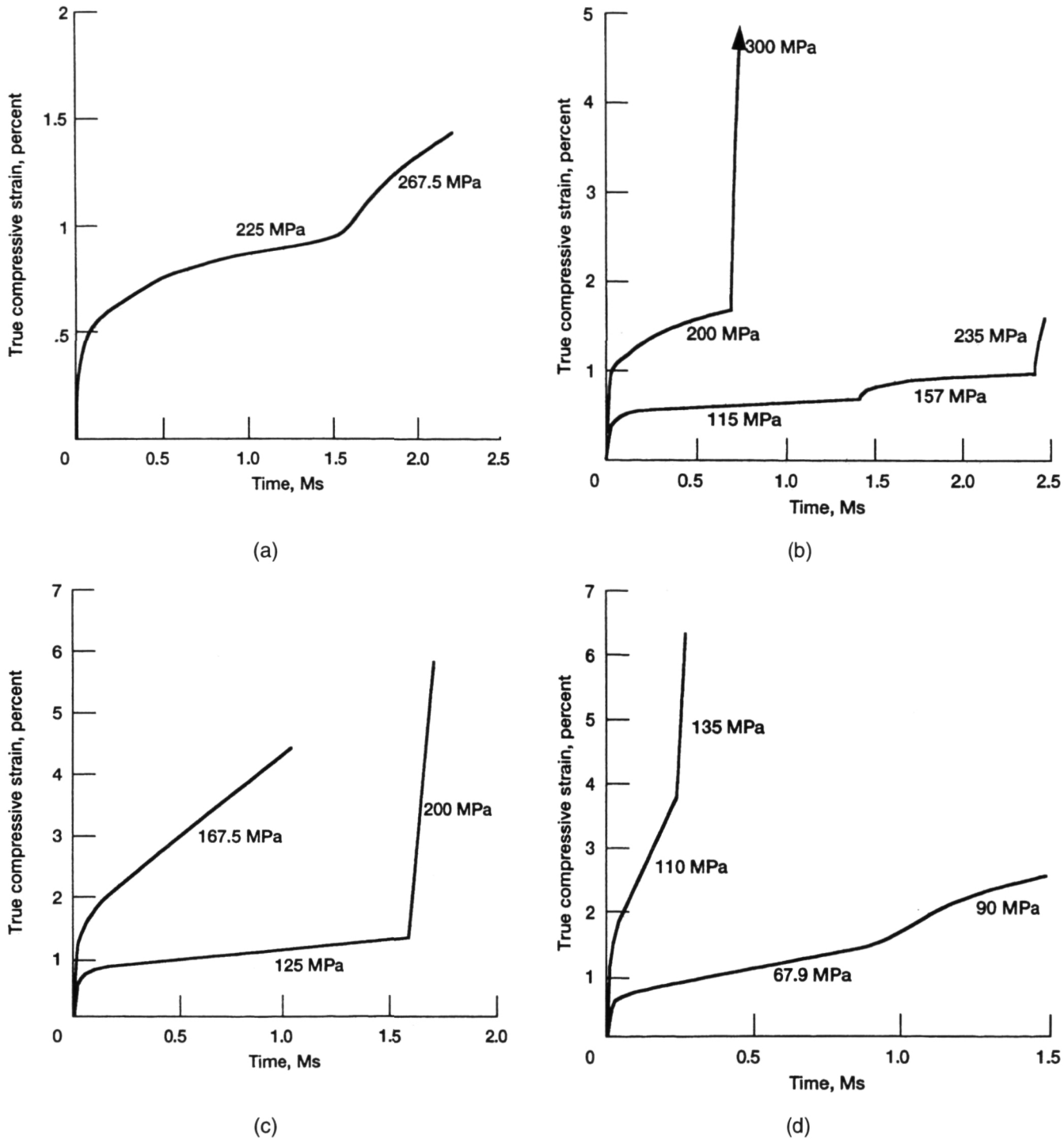

FIG. 8. True compressive creep curves for hot extruded cryomilled NiAl alloy Mit-II as functions of engineering stress and temperature: (a) 1000 K, (b) 1100 K, (c) 1200 K, and (d) 1300 K.

NiAl–AlN had very high activation energies for both the $n = 13.1$ or 5.6 regimes (~670 kJ/mol, Table III), while the current lots showed Q values of about 400 kJ/mol in the high stress exponent regime and ~200 kJ/mol in the $n = 2$ regime. Recent work by Raj and Farmer[17] on polycrystalline NiAl has also reported a high temperature and low stress deformation regime where the stress exponent was ~2; however, the activation energy was only about 96 kJ/mol, which would be indicative of a grain boundary diffusion process. At lower temperatures and higher stresses, they calculated a stress exponent of ~6 and a 290 kJ/mol activation energy, which are both

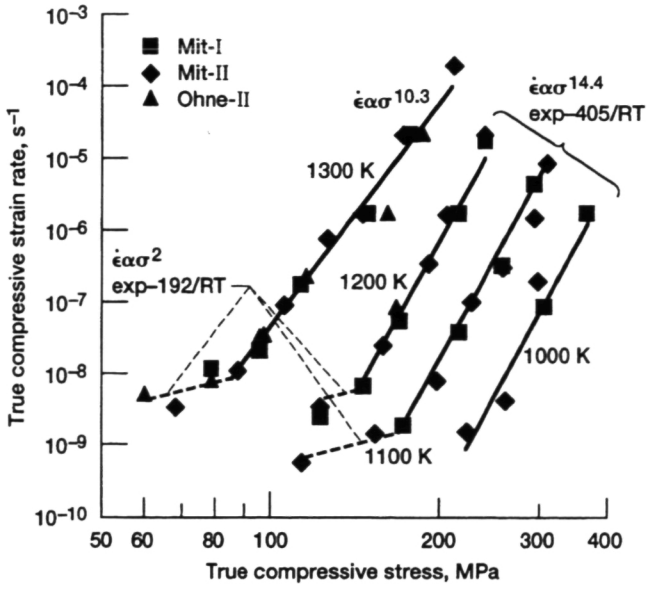

FIG. 9. True compressive flow stress-strain rate behavior for hot extruded cryomilled NiAl as a function of temperature.

typical of dislocation climb controlled creep in NiAl,[16] with Q being associated with a volume diffusion process. Raj and Farmer's activation energy values are both about 100 kJ/mol lower than the estimates for the two deformation regimes in current lots of compression-tested NiAl–AlN (Table III). This, perhaps, indicates that the AlN particles are interfering with grain boundary and volume diffusion processes by inhibiting the operation of vacancy sources/sinks, which results in higher activation energies.

2. Tensile testing

Adequate material was available to machine tensile creep samples from both 76 mm tooling, 12 : 1-1505 K extrusions (Mit-II and Ohne-II) and from the 50 mm tooling 8 : 1-1505 K extrusions of the aluminide cryomilled without yttria (identified as "ohne," Table I) and with Y_2O_3 (identified as "mit," Table I). Results from the constant load testing between 1100 and 1300 K for Mit-II and Ohne-II are given in Figs. 11 and 12, respectively; the creep behavior of mit and ohne at 1300 K was similar to that shown in Figs. 11(c), 11(d), and 12(b). In general the tensile creep curves were typical of most high temperature materials and contained primary, steady state, and tertiary creep regimes. While the majority of the samples exhibited only from 1% to 3% strain at failure, several examples of much greater strains to failure were noted; for instance, the 1100 K, 225 MPa [Fig. 11(a)] and 1300 K, 50 MPa [Fig. 11(d)] tests of Mit-II. Comparison of fracture site to the strain at failure indicated that many, but not all, of the samples exhibiting relatively low ductility failed at or very near the gage to buttonhead transition. Although grinding flaws in the filet region might have contributed to premature fracture in some cases, several examples existed with both low tensile elongation and failure in the reduced section: for instance, Mit-II at 1300 K, 75 MPa [Fig. 11(c)] and Ohne-II at 1200 K, 90 MPa [Fig. 12(a)].

Steady-state creep rates taken from tensile creep curves are shown in Fig. 13 as functions of temperature, stress, and material. As opposed to the compressive results, extrusion reduction ratio appeared to affect the 1300 K strength of the NiAl cryomilled with yttria [Fig. 13(a)], where the 8 : 1 extruded mit is weaker than the 12 : 1 extruded Mit-II. This tendency was not followed, however, by the aluminide that was cryomilled without Y_2O_3 [Fig. 13(b)], where the 8 : 1 extrusion ohne was as strong as the 12 : 1 extrusion Ohne-II. In terms of the deformation parameters of Eq. (1), the 1200 and 1300 K steady-state creep behavior of ohne and Ohne-II can be described by a single stress exponent and activation energy [Table IV(a)]. On the other hand, the deformation of Mit-II divided into two different regimes with high (15.1) and low (6.9) stress exponents and a common activation energy (~600 kJ/mol). The slightly weaker 8 : 1 extruded alloy mit displayed an n value of 6.5 at 1300 K, which is similar to that of the low stress exponent regime of Mit-II. Comparison of the tensile

TABLE III. Temperature-compensated power law fits of true compressive flow stress-strain rate data for several NiAl–AlN alloys tested under constant velocity and constant load creep conditions.

Regime	B (s^{-1})	n	Q (kJ/mol)	R_d^2	δ_n	δ_Q (kJ/mol)
High stress at 1300 K	9.26×10^{-29}	10.3	...	0.973	0.48	...
High stress at 1000–1200 K	1.85×10^{-22}	14.4	404.9	0.964	0.65	20.6
Low stress at 1000–1200 K	6.12×10^{-5}	2.01	191.8	0.896	0.55	27.3
High stress at 1200–1400 K[10]	9.64×10^{-10}	13.1	640.5	0.975	1.1	47.4
Low stress at 1300–1500 K[10]	7.02×10^{21}	5.57	705	0.958	0.29	33.2

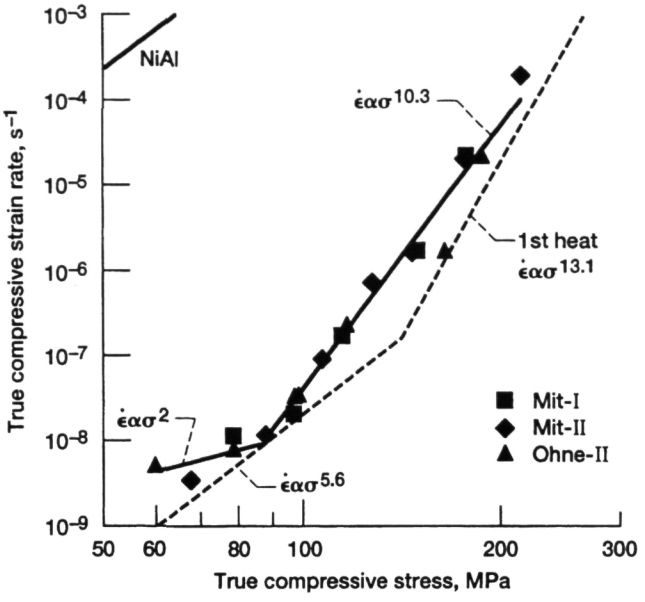

FIG. 10. True compressive 1300 K flow stress-strain rate behavior for current lots of cryomilled NiAl, the first heat of NiAl-AlN,[1–4,10] and polycrystalline NiAl.[16]

creep data for materials cryomilled with/without yttria (Fig. 13) revealed that Ohne-II is considerably weaker than Mit-II at 1200 K, but Ohne-II was only slightly weaker than Mit-II at 1300 K. In fact, the strength of the 12 : 1 extruded Ohne-II and/or 8 : 1 extruded ohne at 1300 K were equivalent to that of the 8 : 1 extruded mit, as use of a dummy variable in conjunction with Eq. (1) failed to reveal any statistically significant differences. Similar testing of the 1300 K data for Mit-II against Ohne-II, ohne, and/or mit indicated that the properties of Mit-II were statistically different from those of the other materials.

The stress rupture properties of cryomilled NiAl are given in Fig. 14. These data have been fitted to

$$t_r = B'\sigma^p \exp\left(\frac{Q_r}{RT}\right), \quad (2)$$

where t_r is the time to rupture, B' is a constant, p is the stress exponent for rupture, and Q_r is the activation energy for rupture. In the case of mit and Mit-II [Fig. 14(a)], the relatively low life (~1000 h) for the sample of mit at 1300 K, 50 MPa suggested that the 1505 K, 8 : 1 extruded material was weaker than the 1505 K, 12 : 1 extruded Mit-II; hence, only the results for this latter alloy were fitted to Eq. (2). On the other hand, the times to failure for ohne and Ohne-II [Fig. 14(b)] were similar, and the data could be described by a single equation. The results from regression fitting to Eq. (2) are shown in Fig. 14 and are given in Table IV(b) along with the standard deviations for the stress exponent (δ_p) and activation energy (δ_{Q_r}) for rupture. Comparison of the two 12 : 1 extruded materials indicated that Ohne-II [Fig. 14(b)] is less resistant to rupture at 1200 K than Mit-II [Fig. 14(a)]. The picture was less clear at 1300 K where the 75 and 100 MPa rupture lives (217.7 and 20.9 h, respectively) for Ohne-II falls on the line describing the behavior of Mit-II [Fig. 14(a)], while the 1015.5 h life for Ohne-II at 50 MPa is much less than the 5587 h life of Mit-II. It is possible that Ohne-II, as well as mit and ohne, suffered premature fracture when tested at 1300 K, 50 MPa, since all three samples failed near the gage to buttonhead transition.

IV. DISCUSSION

The present study of cryomilled NiAl has a number of variables incorporated within the text matrix. In addition to the difference in yttria content, other variables included the stress state (compression versus tension) and the extrusion parameters (tooling size and reduction ratio). Initial compression studies[2,3] of NiAl–AlN indicated that the extrusion ratio might be an important factor governing the creep strength at high temperatures and low strain rates. It was reasoned in Refs. 2 and 3 that the relative weakness of the 8 : 1 extruded stock in comparison to the 12 : 1 extrusion was due to a decrease in the grain aspect ratio (length/diameter) of the cigar-shaped grains. The current 1000 to 1300 K compressive flow stress-strain rate results (Fig. 9) do not support this contention, since the strengths of the 8 : 1 extrusion (Mit-I) are the same as the 12 : 1 extrusion (Mit-II). Furthermore, the 1300 K tensile creep [Fig. 13(b)] and rupture [Fig. 14(b)] behavior of NiAl milled without a yttria addition indicates that the deformation resistance of the 51 mm tooling, 8 : 1 reduction ratio material (ohne) is identical to that of Ohne-II (76 mm tooling, 12 : 1 reduction ratio). On the other hand, the 1300 K tensile flow stress-strain rate properties [Fig. 13(a)] and rupture lives [Fig. 14(a)] of yttria-containing materials do show a dependency on extrusion conditions, where the 51 mm tooling, 8 : 1 reduction ratio material (mit) is slightly weaker than Mit-II (76 mm tooling, 12 : 1 reduction ratio). In total the current work cannot unilaterally confirm or deny grain aspect ratio effects in extruded NiAl–AlN; however, the present results do suggest that the differences in creep strength between 8 : 1 and 12 : 1 extrusions are small at best. The overall question regarding the influence of grain structure could probably be best answered through comparison of tensile creep properties of lots of NiAl–AlN that have been densified by hot isostatic pressing and extrusion at the same temperature.

A. Stress state

The absolute values of flow stresses and steady-state creep rates for the current NiAl–AlN tested in compression and tension are compared in Fig. 15 as

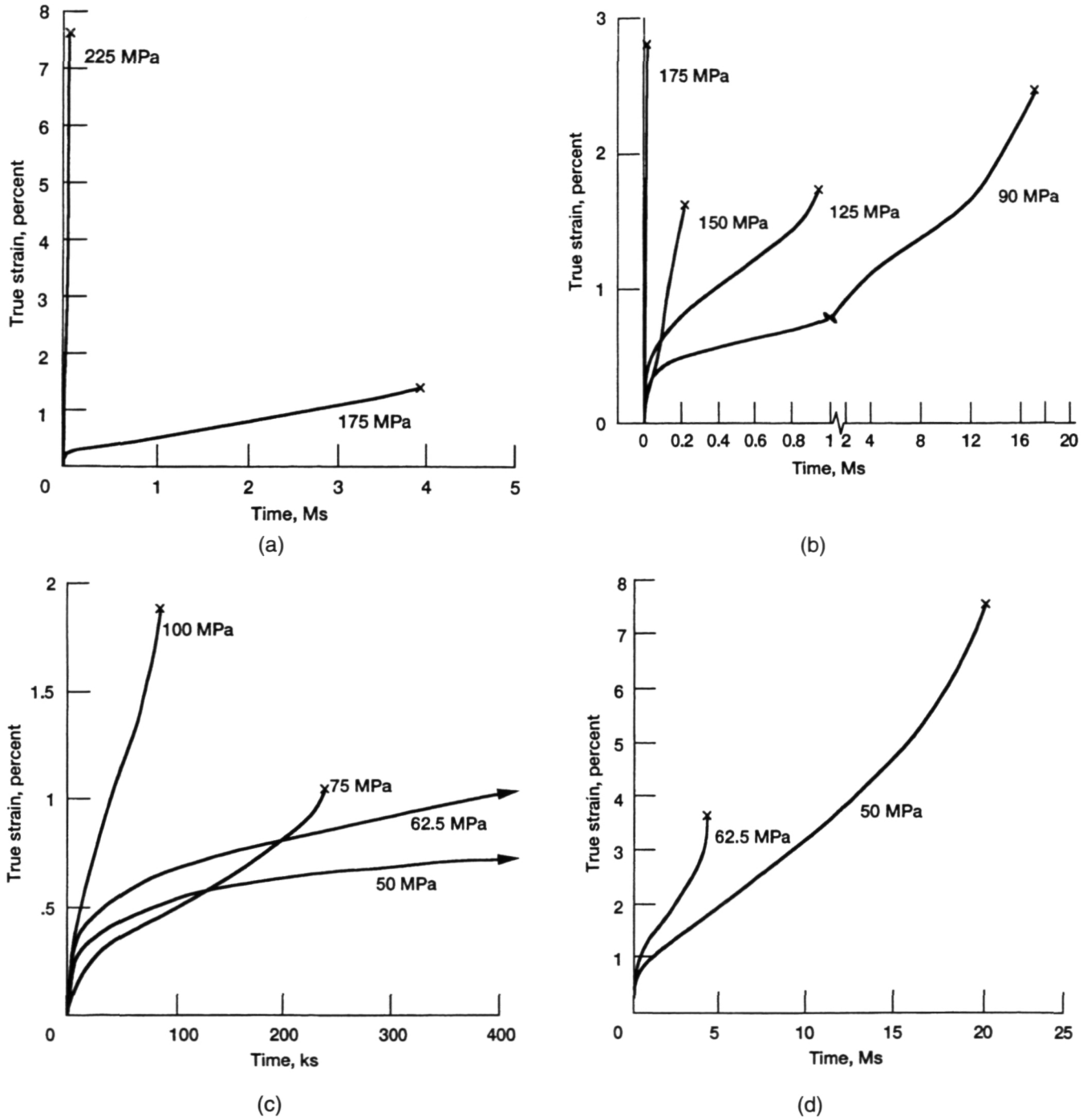

FIG. 11. True tensile creep curves for hot extruded cryomilled NiAl alloy Mit-II as functions of engineering stress and temperature: (a) 1100 K, (b) 1200 K, and (c, d) 1300 K.

a function of temperature, where only the experimental data for Mit-II are plotted. While the curves delineating the tensile test results are solely for Mit-II [Fig. 13(a)], the lines describing the compressive behavior are from the combined lot of Mit-I, Mit-II, and Ohne-II (Fig. 9). Figure 15 illustrates two points: (i) Tensile-tested NiAl–AlN seems to be weaker in tension than compression at 1200 and 1300 K, but the dependency on the stress state appears to be small, or nonexistent, at 1100 K; and (ii) based on the 1200 and 1300 K results, the change in deformation mechanism suggested by compression testing ($n \approx 12$ to $n \approx 2$) is not reflected in the tensile behavior. In fact, the power-law description of the tensile results for Mit-II (Table IV) have more in common with the power-law parameters for the original lot of NiAl–AlN (Table III, Ref. 10)

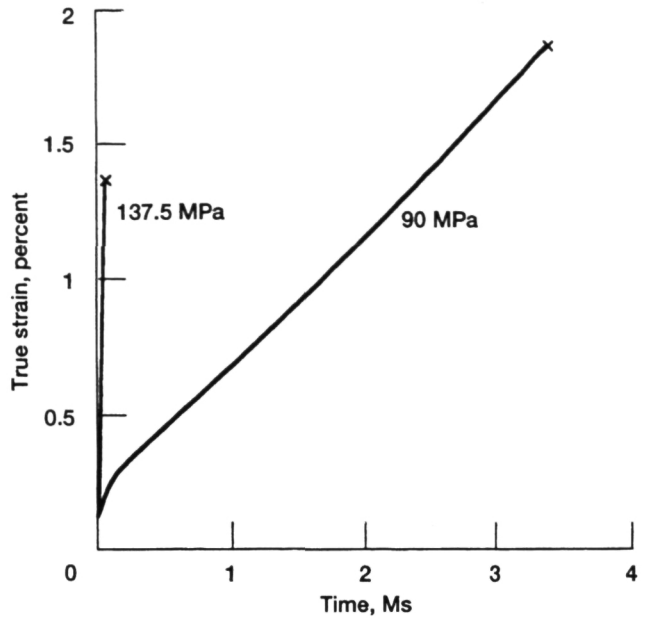

(a)

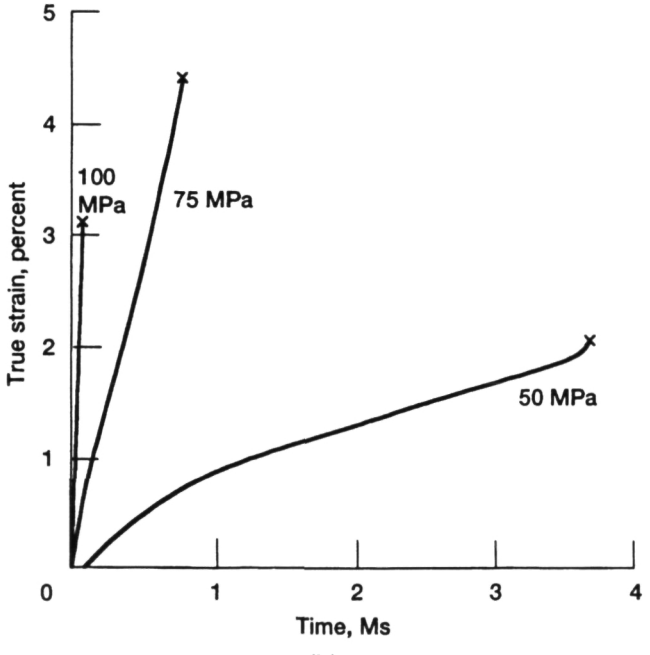

(b)

FIG. 12. True tensile creep curves for hot extruded cryomilled NiAl alloy Ohne-II as functions of engineering stress and temperature: (a) 1200 K and (b) 1300 K.

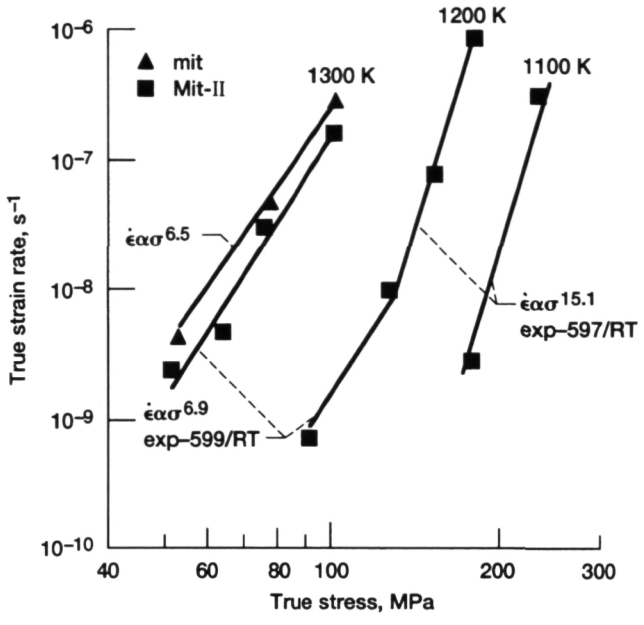

(a)

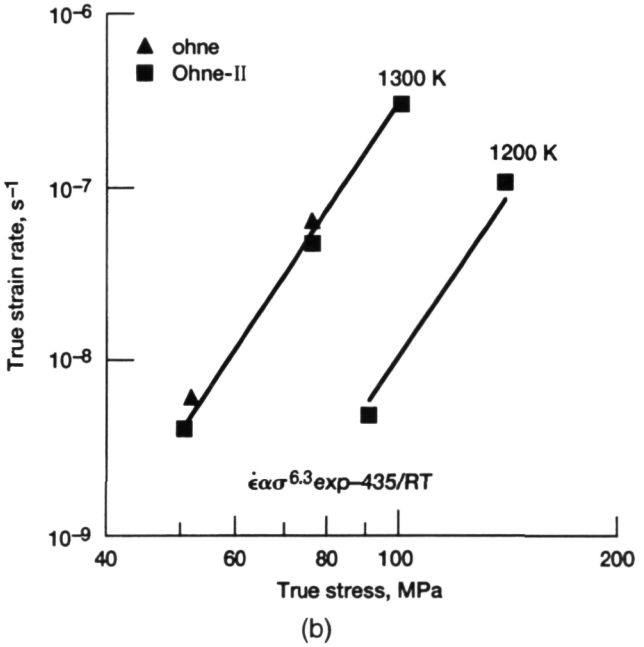

(b)

FIG. 13. True tensile steady state stress-strain rate behavior for hot extruded cryomilled NiAl as a function of temperature. (a) NiAl cryomilled with yttria and (b) NiAl cryomilled without yttria.

than those for compression tested Mit-II (Table III). For example, Mit-II in tension exhibits stress components of ~15 and ~7 combined with a ~600 kJ/mol activation energy; the first lot of NiAl–AlN in compression had n values of ~13 and ~6 couples with a Q of ~670 kJ/mol, but Mit-II in compression exhibited two vastly different regimes: $n = 14.4$ and $Q = 405$ kJ/mol at higher stresses, lower temperatures and $n = 2$ and $Q = 192$ kJ/mol at lower stresses, higher temperatures. Possibly the low stress exponent–low activation energy regime in compression-tested lots Mit-I, Mit-II, and Ohne-II is an artifact due to overestimates of the steady-state creep rate [in general, the compressive creep tests with rates $< 10^{-8}$ s^{-1} were conducted only for ~1.5 Ms (Fig. 8) while the tensile creep tests ran for 3^{+} Ms (Fig. 11)] or simply a mathematically correct set of parameters with no physical meaning.

TABLE IV. Temperature-compensated power law fits for several NiAl–AlN alloys tested under constant load tensile creep conditions.

(a) True flow stress-strain rate data

Material	B (s^{-1})	n	Q (kJ/mol)	R_d^2	δ_n	δ_Q (kJ/mol)
Ohne-II and ohne 1200–1300 K	2.20×10^{-2}	6.32	435.4	0.987	0.36	34.2
Mit-II, High stress at 1100–1200 K	1.44×10^{-14}	15.1	596.7	0.974	1.8	78.5
Mit-II, Low stress at 1200–1300 K	3.38×10^{3}	6.88	599.1	0.974	0.73	59.8
Mit at 1300 K	2.97×10^{-20}	6.48	...	0.999	0.09	...
Ohne-II, ohne, and mit, 1200–1300 K	8.87×10^{-3}	6.32	426.8	0.989	0.25	25.9

(b) Engineering stress–time to failure data

Material	B' (h)	p	Q_r (kJ/mol)	R_d^2	δ_p	δ_{Q_r} (kJ/mol)
Mit-II 1100–1300 K	8.77×10^{-3}	−8.66	514.0	0.907	1.06	79.6
Ohne-II and ohne 1200–1300 K	0.52	−6.47	360.0	0.940	0.88	85.6

Currently, extensive transmission electron microscopy (TEM) of both compression-and tensile-tested Mit-II is being undertaken to determine if the changes in stress exponent and/or activation energy are accompanied by differences in the dislocation structure. Preliminary TEM studies[18] of another lot of NiAl–AlN, which shows a stress exponent transition from ~13 to ~6, have revealed different structures in the AlN-free grains. Specifically, high dislocation density, cold worklike configurations are found in the $n \approx 13$ regime, while subboundaries with internal networks are seen after deformation of samples exhibiting the $n \approx 6$ mechanism.

B. Yttria content

Although the original concept of this study was to produce two lots of AlN particulate reinforced NiAl that varied only in yttria level, identical cryomilling techniques (Table I) did not yield the desired result. Hence, the tested materials varied in their matrix chemistries and second phase content (AlN, Al_2O_3, and Y_2O_3). Based on previous work,[16] the 1 at. % difference in Al level (47.5 vs 46.5) will not affect elevated temperature strength; in addition, it has been shown that alumina does not provide any effective high temperature deformation resistance in NiAl.[7] Therefore, any differences in mechanical behavior due to composition should be ascribed to the AlN + Y_2O_3 content.

Comparison of the creep properties for the 76 mm tooling, 12 : 1 extruded materials (Mit-II with 8.1 vol % AlN and 0.5 vol % Y_2O_3 versus Ohne-II with 10.5 vol % AlN) provides the most extensive basis to examine the influence of AlN + Y_2O_3 content. Based on the compressive flow stress-strain rate data in Fig. 9, little real difference in strength exists between Mit-II and Ohne-II. The tensile results (Figs. 13 and 14), however, indicate that Mit-II is stronger than Ohne-II. Although only two 1200 K tensile creep tests were conducted for Ohne-II, their rupture lives [Fig. 14(b)] were significantly below that of Mit-II [Fig. 14(a)], and their creep rates [Fig. 13(b)] were larger than those of Mit-II [Fig. 13(a)]. At 1300 K, the difference between these two materials is much smaller, where, for identical test conditions, the tensile creep rate of Ohne-II is about twice that for Mit-II and the rupture lives were similar except for the 50 MPa tests. Comparison of the 1300 K behavior of the two 51 mm tooling, 8 : 1 extrusions (mit and ohne) in terms of their flow stress-strain rate properties (Fig. 13) and rupture lives (Fig. 14) also reveals similar characteristics.

As the compressive results indicate no difference between Mit-II and Ohne-II and the tensile data imply that the lot of NiAl cyromilled with yttria is stronger than the lot cryomilled without Y_2O_3, it is not possible to argue that the elevated temperature strength of NiAl–AlN increases with a change of nitride content from 8 to 10.5 vol %. This conclusion is reinforced by similar results[9] for several lots of NiAl–AlN that contained from 11 to 14 vol % AlN and, yet, possessed statistically identical 1300 K compressive properties. Thus, while a general trend of increasing strength with AlN content exists in nitride strengthened NiAl,[10] little difference in behavior can be expected when the AlN varies within a ~20 relative percent range. Lastly, the inability to separate differences in elevated temperature strength properties based on small changes in AlN level negates any attempt to understand the role of yttria. All that can be stated with certainty is that the presence of Y_2O_3 in

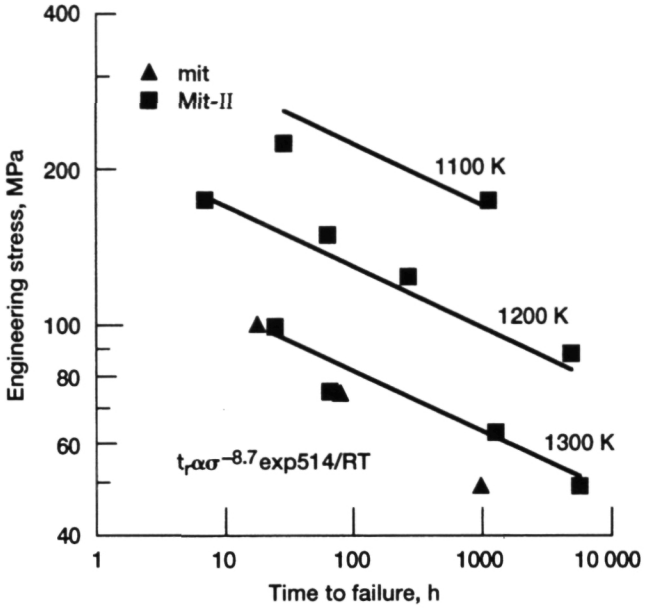

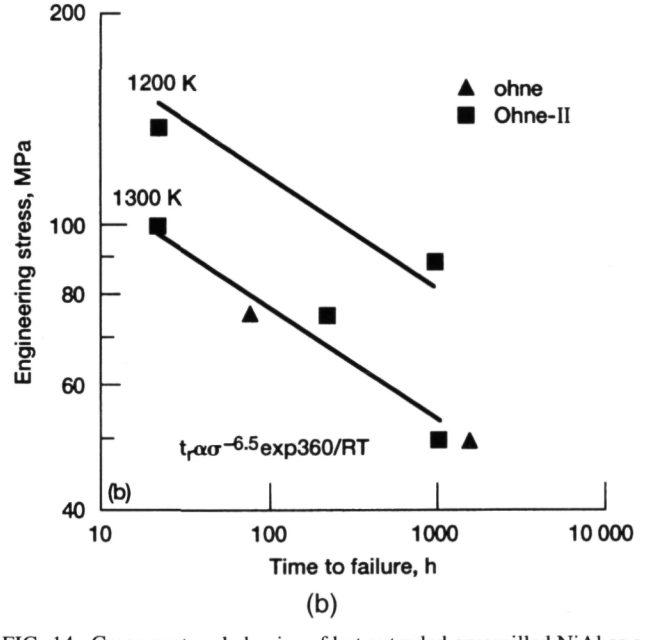

FIG. 14. Creep rupture behavior of hot extruded cryomilled NiAl as a function of temperature. (a) NiAl cryomilled with yttria and (b) NiAl cryomilled without yttria.

NiAl–AlN is very beneficial for oxidation resistance,[10,15] and it is not detrimental with regard to mechanical behavior.

C. Comparison of elevated temperature strengths

Since its discovery,[1] cryomilling of NiAl has been suggested as a means to produce strong high temperature NiAl-based materials capable of supplanting superalloys. With the current report of tensile creep properties for

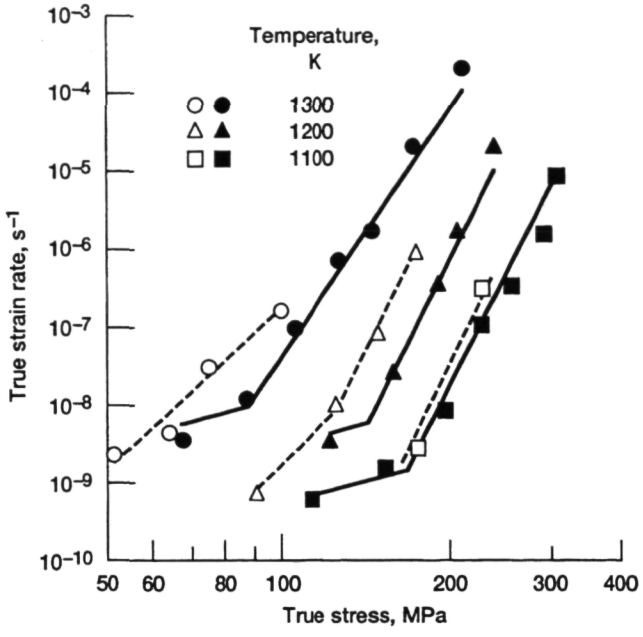

FIG. 15. Comparison of tensile (open symbols) and compressive (solid symbols) steady-state stress-strain rate behavior for hot extruded NiAl cryomilled with yttria (Mit-II) as a function of temperature.

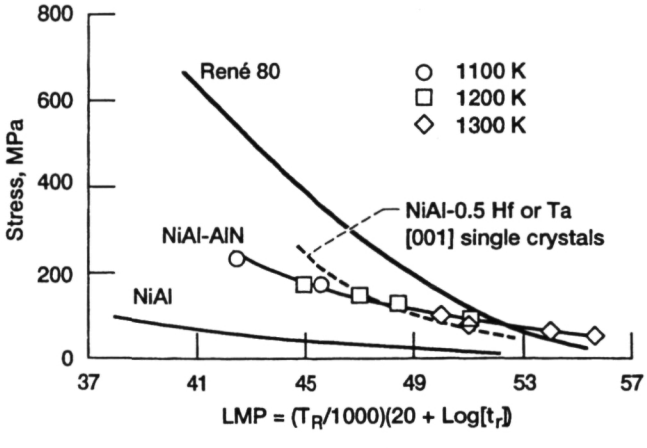

FIG. 16. Larson–Miller representation of the creep rupture behavior of polycrystalline NiAl,[19] NiAl–0.5Hf, and NiAl–0.5Ta single crystals,[20] René 80,[19] and NiAl–AlN (Mit-II).

NiAl–AlN, this contention can be tested by use of the Larson–Miller parameter (LMP), where

$$\mathrm{LMP} = \left(\frac{T_R}{1000}\right) \times (20 + \log_{10} t_r) \qquad (3)$$

and, following tradition, the test temperature T_R is in °R. Utilization of the engineering stress as a function of LMP (Fig. 16) then allows a ready contrast of the rupture behavior of NiAl–AlN (Mit-II) to polycrystalline NiAl, NiAl–0.5Hf, and NiAl–0.5Ta [001] single crystals and the Ni-base superalloy René 80. Clearly the cyromilled NiAl is much stronger than its polycrystalline matrix and nearly equally as strong as either Hf- or Ta-containing

NiAl single crystals; however, only under long-term, high-temperature conditions does NiAl–AlN show some superiority over René 80.

As data in Fig. 16 suggest, the inferiority of NiAl–AlN to René 80 is basically a result of the lack of strength at 1100 and 1200 K. Thus it is likely that cryomilling of NiAl-containing minor (~1%) alloying additions of Hf, Ta, Zr, etc. could greatly improve behavior, as these elements provide significant solid solution and precipitation hardening at lower temperatures.[2] While significant increases in the AlN content will also strengthen,[10] sufficient improvement to the stress-LMP numbers of René 80 (Fig. 16) is probably not possible with a binary matrix. Furthermore, high AlN contents via cryomilling make it more difficult for high matrix Al levels to be maintained, which, in turn, could lower the oxidation resistance. It is our present belief that third element additions to the NiAl matrix will be necessary to obtain superalloy level elevated temperature mechanical properties in NiAl–AlN based materials.

V. SUMMARY AND CONCLUSIONS

As part of a program to assess the influence of yttria on the behavior of AlN particulate strengthened NiAl produced by cryomilling, the elevated temperature creep properties of NiAl–AlN with and without Y_2O_3 have been determined both in compression and in tension as functions of stress, temperature, and extrusion condition. Significant findings in this study include: (i) Similar compressive creep strengths were measured for both materials, but tensile creep rupture testing indicated that the yttria-containing alloy was slightly stronger than the Y_2O_3-free version. (ii) Compression and tensile testing showed both high and low stress exponent regimes; in compression the latter mechanism had a very low stress exponent (2) in combination with a small activation energy (200 kJ/mol). (iii) Small differences in AlN content and/or extrusion ratio do not significantly affect elevated temperature strength. (iv) Comparison of the LMP to other materials indicates that NiAl–AlN has long term, high-temperature strength at least equal to conventional superalloys.

The present work reinforces previous contentions that cryomilling can produce strong aluminum nitride reinforced NiAl with the potential for elevated temperature structural applications. It is also clear from the LMP analysis that strengthening of the matrix by alloying will be required for NiAl–AlN to exceed the properties of conventional superalloys at intermediate temperatures.

ACKNOWLEDGMENT

The authors would like to acknowledge Dr. B. J. M Aikin for providing the laser light size/distribution results for the as-cryomilled powders.

REFERENCES

1. J. D. Whittenberger, E. Arzt, and M. J. Luton, J. Mater. Res. **5**, 271 (1990).
2. J. D. Whittenberger, E. Arzt, and M. J. Luton, in *Intermetallic Matrix Composites,* edited by D. L. Anton, P. L. Martin, D. B. Miracle, and R. McMeeking (Mater. Res. Soc. Symp. Proc. **194**, Pittsburgh, PA, 1990), pp. 211–217.
3. J. D. Whittenberger, E. Arzt, and M. J. Luton, J. Mater. Res. **5**, 2819 (1990).
4. J. D. Whittenberger, E. Arzt, and M. J. Luton, Scripta Metall. et Mater. **26**, 1925 (1992).
5. J. D. Whittenberger and M. J. Luton, J. Mater. Res. **7**, 2724 (1992).
6. T. R. Bieler, R. D. Noebe, J. D. Whittenberger, and M. J. Luton, in *Intermetallic Matrix Composites II,* edited by D. B. Miracle, D. L. Anton, and J. A. Graves (Mater. Res. Soc. Symp. Proc. **273**, Pittsburgh, PA, 1992), pp. 165–170.
7. M. G. Hebsur, J. D. Whittenberger, R. M. Dickerson, and B. J. M. Aikin, in *High Temperature Ordered Intermetallic Alloys V,* edited by I. Baker, R. Darolia, J. D. Whittenberger, and M. H. Yoo (Mater. Res. Soc. Symp. Proc. **288**, Pittsburgh, PA, 1993), pp. 1111–1116.
8. T. R. Bieler, J. D. Whittenberger, and M. J. Luton, in *High Temperature Ordered Intermetallic Alloys V,* edited by I. Baker, R. Darolia, J. D. Whittenberger, and M. H. Yoo (Mater. Res. Soc. Symp. Proc. **288**, Pittsburgh, PA, 1993), pp. 1149–1154.
9. B. J. M. Aikin, J. D. Whittenberger, and M. G. Hebsur, *Mechanical Alloying for Structural Applications,* edited by J. J. deBarbadillo, F. H. Froes, and R. Schwarz (ASM INTERNATIONAL, Materials Park, OH, 1993), pp. 283–290.
10. J. D. Whittenberger, in *Structural Intermetallics,* edited by R. Darolia, J. J. Lewandowski, C. T. Liu, P. L. Martin, D. B. Miracle, and M. V. Nathal (TMS, Warrendale, PA, 1993), pp. 819–828.
11. M. J. Luton, C. S. Jayanth, M. M. Disko, S. Matras, and J. Vallone, in *Multicomponent Ultrafine Microstructures,* edited by L. E. McCandlish, D. E. Polk, R. W. Siegel, and B. H. Kear (Mater. Res. Soc. Symp. Proc. **132**, Pittsburgh, PA, 1989), pp. 79–86.
12. Benlih, J. Vallone, C. F. Klein, and M. J. Luton, in *Intermetallic Matrix Composites II,* edited by D. B. Miracle, D. L. Anton, and J. A. Graves (Mater. Res. Soc. Symp. Proc. **273**, Pittsburgh, PA, 1992), pp. 171–176.
13. B. J. M. Aikin, R. M. Dickerson, D. T. Jayne, S. Farmer, and J. D. Whittenberger, Scripta Metall. et Mater. **30**, 119–122 (1994).
14. C. E. Lowell, C. A. Barrett, and J. D. Whittenberger, in *Intermetallic Matrix Composites,* edited by D. L. Anton, P. L. Martin, D. B. Miracle, and R. McMeeking (Mater. Res. Soc. Symp. Proc. **194**, Pittsburgh, PA, 1990), pp. 355–360.
15. C. E. Lowell and C. A. Barrett, unpublished research, NASA Lewis Research Center, Cleveland, OH.
16. J. D. Whittenberger, J. Mater. Sci. **22**, 394 (1987).
17. S. V. Raj and S. F. Farmer, in *High Temperature Ordered Intermetallic Alloys V,* edited by I. Baker, R. Darolia, J. D. Whittenberger, and M. H. Yoo (Mater. Res. Soc. Symp. Proc. **288**, Pittsburgh, PA, 1993), pp. 647–652.
18. A. Garg, J. D. Whittenberger, and B. J. M. Aikin, in *Intermetallic Matrix Composites III,* edited by J. A. Graves, R. R. Bowman, and J. J. Lewandowski (Mater. Res. Soc. Symp. Proc. **350**, Pittsburgh, PA), pp. 231–236.
19. R. Darolia, JOM **43** (3), 44 (1991).
20. W. S. Walston, R. D. Field, J. R. Dobbs, D. F. Lahrman, and R. Darolia, in *Structural Intermetallics,* edited by R. Darolia, J. J. Lewandowski, C. T. Liu, P. L. Martin, D. B. Miracle, and M. V. Nathal (TMS, Warrendale, PA, 1993), pp. 523–532.
21. R. D. Noebe, R. R. Bowman, and M. V. Nathal, Int. Mater. Rev. **38**, 193 (1993).